Liu *et al. Int J Concr Struct Mater* (2022) 16:36
https://doi.org/10.1186/s40069-022-00527-7

International Journal of Concrete Structures and Materials

RESEARCH Open Access

Post-fire Bond Behaviors Between Grout and Steel Rebar

Liang-Lin Liu*, Chun-Yong Luo, Lu-Xia Ouyang, Zhen-Hua Xia and Wei-Hua Li

Abstract

Firstly, according to the theoretical analysis, the force mechanism and failure modes were assured for the bond behavior between grout and steel rebar. Then, a pull-out experiment was exerted to probe the bond behavior developments of specimens after exposed to 500 °C. It is found that the mixed measures of pre-drying and slow elevating rate, i.e., 5 °C/min, inhibits the explosive spalling in grout with compressive strength of 76.7 MPa. In addition, there are two failure modes including the steel rebar fracture and the bond slip failure in the test. Based on the elevated temperature, compressive strength of post-fire grout, diameter of steel rebar and its embedment length, a new expression has been built to calculate the bond strength between grout and steel rebar of post-fire specimens. Furthermore, the finite element simulation is employed to investigate the bond behaviors of pull-out specimens after exposed to elevated temperatures up to 500 °C. The steel rebar fracture is captured firstly in the pull-out test simulation. Moreover, it is found that the peak slips increase and peak loads decrease along with the temperature elevating. Finally, it is proposed that the crucial elevated temperatures of the failure mode change should be 300, 300 and 400 °C for the specimens with embedment lengths of 6, 7 and 8 times diameter of steel rebar with diameter of 16 mm, respectively, which is beneficial for evaluating the fire safety of the existing structure elements.

Keywords: pull-out test, force mechanism, elevated temperature, simulation analysis, failure mode

1 Introduction

Nowadays, based on the advantages of reliable mechanical behaviors, wide adaptability and easy installation, the grouted sleeve connection became to the mainstream method for steel rebar splicing in precast concrete structures (Zhang et al., 2018). Application of the connection technology could accelerate the speed of erection, significantly reduces required rebar lap length, and guarantees higher quality assurance (Ling et al., 2008). According to the mechanical behaviors of the connection were not less than these of the connected rebars, the steel rebar fracture outside the sleeve could be defined as a required failure mode, which enhanced the reliability of the connection. It was found that the reliability of the connection mainly depended on the bond strengths of grout-to-sleeve and grout-to-rebar (Zheng et al., 2016). As the most important performance of the grouted sleeve connection, the bond strength between grout and steel rebar affected the structural performance of precast concrete structures with grouted sleeve connections significantly (Hosseini & Rahman, 2016; Kim, 2012). It has been found that the bond strength increased almost proportionally with the increment of grout compressive strength and enhanced by the use of spliced rebar and spiral with small diameter (Hosseini & Rahman, 2016; Liu et al., 2020; Zhang et al., 2018; Zhu et al., 2021). Through multiple regression analysis on the collected data, an equation has been built to calculate the confining pressure from sleeve by Kim (2012), which was used to estimate the bond strength between grout and steel rebar. Moreover, according to the pull-out test results, an expression has been fitted to calculate the bond strength between grout

Journal information: ISSN 1976-0485 / eISSN 2234-1315

*Correspondence: tlliu@tongji.edu.cn

School of Architecture and Civil Engineering, Jinggangshan University, 343009 Ji'an, Jiangxi, China

and steel rebar based on the grout compressive strength, rebar diameter and the embedment length of rebar (Liu et al., 2021). However, these researches only focused on the bond behaviors of grout and rebar at ambient temperature, and little investigation was reported on the force mechanism between grout and steel rebar.

Fire is the common and frequent disaster threatening the public safety. It is well-known that elevated temperatures degrade the mechanical behaviors of materials and loosen the micro-structure of cement-based materials especially, which decrease the bond strength between steel rebar and cementitious material. Therefore, based on the prementioned results at ambient temperature (Liu et al., 2021), the present paper focused on the elevated temperature effects on the bond behaviors of grout and steel rebars by a pull-out test and formed an equation of bond strength between grout and steel rebar by taking elevated temperature into account. Then, a finite element method with Abaqus soft was exerted to simulate the pull-out test specimens after exposed to elevated temperatures. After verification by the results of test, the simulation method was further used to investigate bond behaviors of post-fire specimens in the pull-out test, i.e., the critical temperature of failure mode change, which would be beneficial for evaluating fire safety of the existed structures. Therefore, a theory analysis was used to find out the failure mode types firstly by determining the force mechanism between grout and steel rebar when the pull-out specimen was under incremental tension. Thus, the bond behaviors of grout and steel rebar from post-fire specimens were investigated by combined methods of theory analysis, pull-out test and simulation in the present paper, which would be helpful to forming the method for calculating bearing capacity of grouted sleeve connections and evaluating the fire safety of existing structure elements.

2 Force Mechanism Between Grout and Steel Rebar

Taking the pull-out test for example, it was found that the force mechanism between grout and steel rebar was influenced by three features, i.e., compression between grout and rib of steel rebar, restraint of loading setup and lateral restraint.

2.1 Compression Between Grout and Rib of Steel Rebar

Configurations of pull-out specimens are shown in Fig. 1a, and include two parts, i.e., grout cubic block and steel rebar. When the tension F is applied to the loading end of the rebar, the rib extrudes grout and forms a resultant force R on the surface of rib as shown in Fig. 1b. The resultant force R could be divided into the longitudinal component named R_h and the normal component named R_p. The R_h constitutes the shear stress or bond stress between the grout and steel rebar, which is balanced by the bond strength that consisted of chemical bond action, friction and mechanical interlocking. In addition, the R_p causes the mutual separation between grout and steel rebar and leads to circumferential tensile stress f_{fl} in the grout cubic block, which is balanced by the tensile strength of grout, as shown in Fig. 1c. In addition, the chemical bond action and the friction were affected, i.e., weaken and even vanish, by the mutual separation, which also decreased the efficient shear area on the ribs (Ling et al., 2008). Finally, the only residual part is the mechanical interlocking to form bond strength to balance the shear stress. Therefore, the bond bearing capacity between grout and steel rebar decreases.

2.2 Restraint of Loading Setup

It is well-known that specimens are located at a steel plate of loading setup in the pull-out test (Eligehausen et al., 1983; Li et al., 2004; Xiao et al., 2009), as shown in Fig. 2a. Then, the steel rebar was gone through the hole reserved in the middle of the steel plate, and its bottom was fixed as the loading end. There is uniform pressure q on the surface of grout cubic block from support of the steel plate, which is used to balance the load from loading end of steel rebar as shown in Fig. 2b. The pressure q combined with R_h squeeze the grout along the longitudinal direction, which brings about the grout in the range of steel rebar embedment length under compression. Under the Poisson's ratio effects, the grout is close to the surface of the steel rebar, which enhances the bond strength between grout and steel rebar. Furthermore, the mutual separation of grout and steel rebar is inhibited to a certain degree by the friction f from the contact of grout cubic block and the steel plate, which means that restraints are imposed to the lateral side of cubic block as exhibited in Fig. 2c. Therefore, the grout is under compression from longitudinal and lateral side of cubic block when the block is installed directly to the top of a steel plate in the loading setup, which increases the bond strength between grout and steel rebar and is used to form the stress state of grout in the later finite element simulation analysis.

2.3 Lateral Restraint

The mutual separation between grout and steel rebar is inhibited by the lateral restraint in the form of surface pressure p_1 and (or) p_2 as shown in Fig. 3a or wrapping by FRP (Tastanil & Pantazopoulou, 2010; Xu et al., 2012), or the rebar and grout with sleeve embedding into the structural specimens, i.e., beams (Zhou et al., 2017), as shown in Fig. 3b. Therefore, the bond strength is enhanced by the lateral restraint increasing the interfacial friction

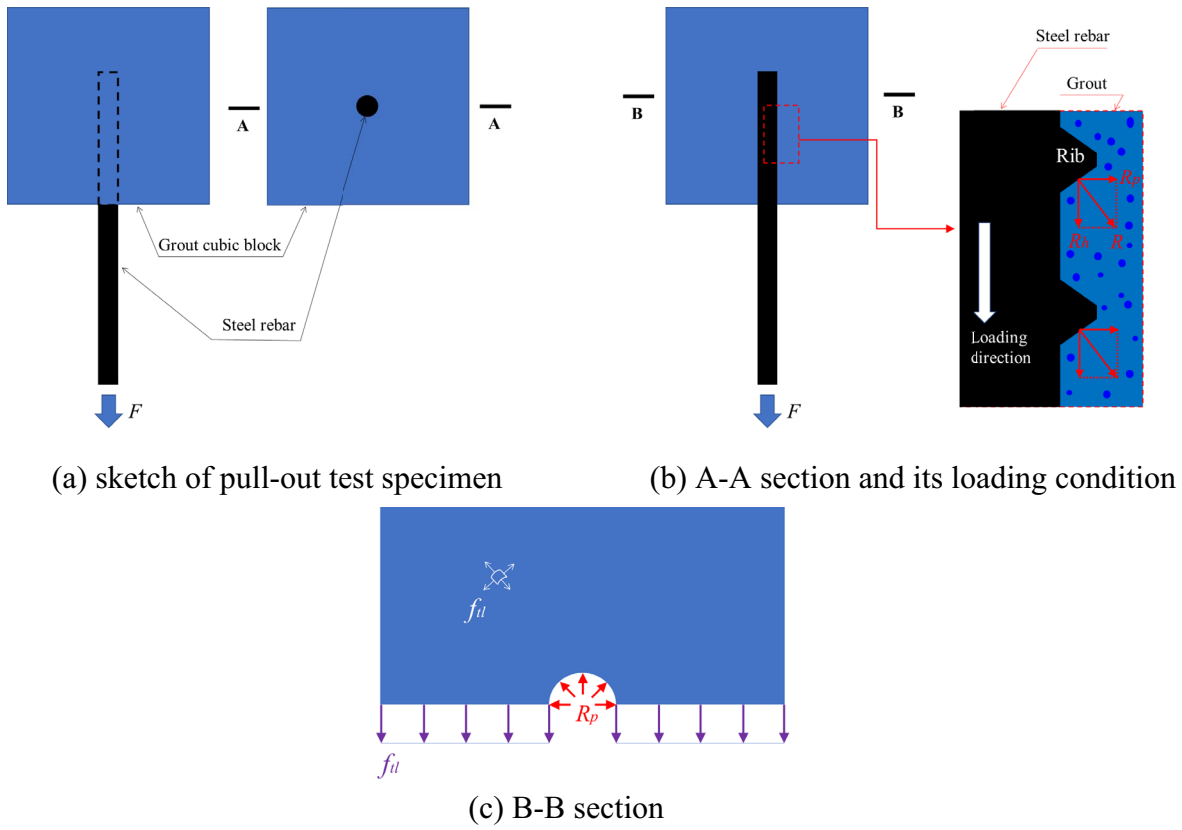

Fig. 1 Force mechanism between grout and steel rebar.

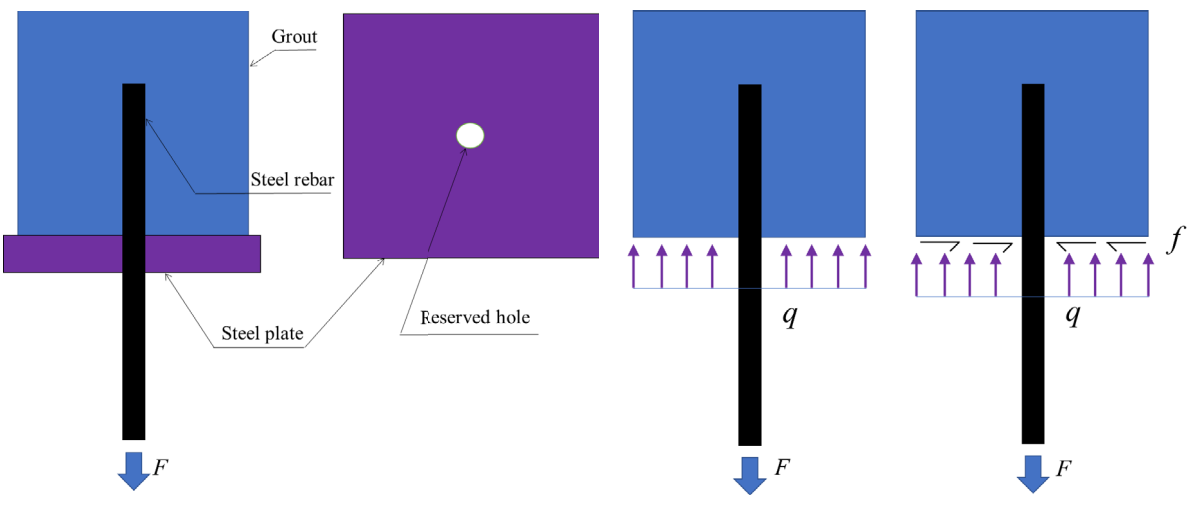

Fig. 2 Effects of loading setup.

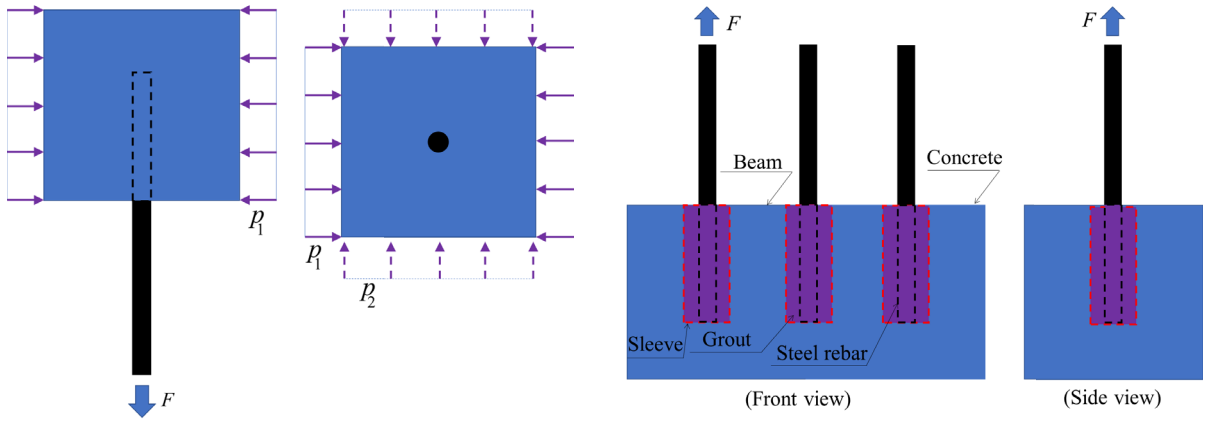

(a) lateral compressive stress (b) restrain of sleeve

Fig. 3 Effects of lateral restraint.

and shear area on the top of ribs. The external load F is delivered into the internal position of grout till the end of embedment length of rebar by the bond strength, and then is balanced by the tensile strength of the grout in the part of specimen without steel rebar. Thus, the force mechanism of pull-out test specimen would be different corresponding to the specimens under different loading regimes and restraining conditions.

2.4 Failure Modes

Based on above-mentioned force mechanisms, it was found that the failure modes of pull-out test specimens should contain the following types. The first one is the split characterized by the longitudinal cracks along with the lateral surfaces of the grout cubic block as exhibited in Fig. 4a. The longitudinal cracks derive from the development of transversal surface cracks caused by the circumferential tensile stress beyond the tensile strength of grout when the external load F increases. Then, the steel rebar is pulled out from the grout cubic block and pumping area is left in the cubic block, and the test is terminated. The second one is the bond slip failure mode characterized by the grout adhered to the steel rebar together being pulled out of the grout cubic block as shown in Fig. 4b. The adhering grout is from the grout keys sheared off among steel rebar ribs when the external load is continuing increasing till the peak load, which breaks the mechanical interlocking. Then, the steel rebar with the sheared-off grout keys is pulled out of the grout cubic block slowly and a pumping area is also left in the cubic block. The third one is the steel rebar fracture characterized by the steel rebar breaks outside the grout cubic block as shown in Fig. 4c. The steel rebar fracture means that the bond bearing capacity between grout and steel rebar is larger than the tensile bearing capacity of the steel rebar, and is a required failure mode in the practical engineering. There was a special failure mode naming plug failure by Zhou et al. (2017) as shown in Fig. 4d. The plug failure may occur during the pull-out test without steel plate upon the loading ending of steel rebar when the steel rebar is bonded by the high-strength cementitious material and the low-strength cementitious material is bonded by the high one, which means that the steel rebar is in the core of the specimen, the high-strength cementitious material like grout is the middle part of specimen and the low one like common concrete is outside of the specimen. Based on the wedging effect of ribs, the steel rebar with cone grout close to the loading end of rebar is pulled out of the grout cubic block when the result force R is larger than the resisted punching shear capacity of oblique section along with the normal direction of rib slope in the grout cubic block. In pace with the pulling out of steel rebar, there is also a pumping area leaving in the residual grout cubic block as shown in Fig. 4d.

3 Bond Behaviors of Post-fire Specimens by Pull-out Tests

3.1 Effects of Elevated Temperature

Mechanical behaviors of cement-based material were affected by the elevated temperature. It has been found that the compressive strength of grout decreased along with the temperature elevating (Zhang et al., 2018), which had obvious effects on the bond strength between grout and steel rebar. As the water evaporated, the pores and capillary cracks were left in the grout after exposed to elevated temperature, which was investigated by the scanning electron microscope method (Zhu et al., 2020).

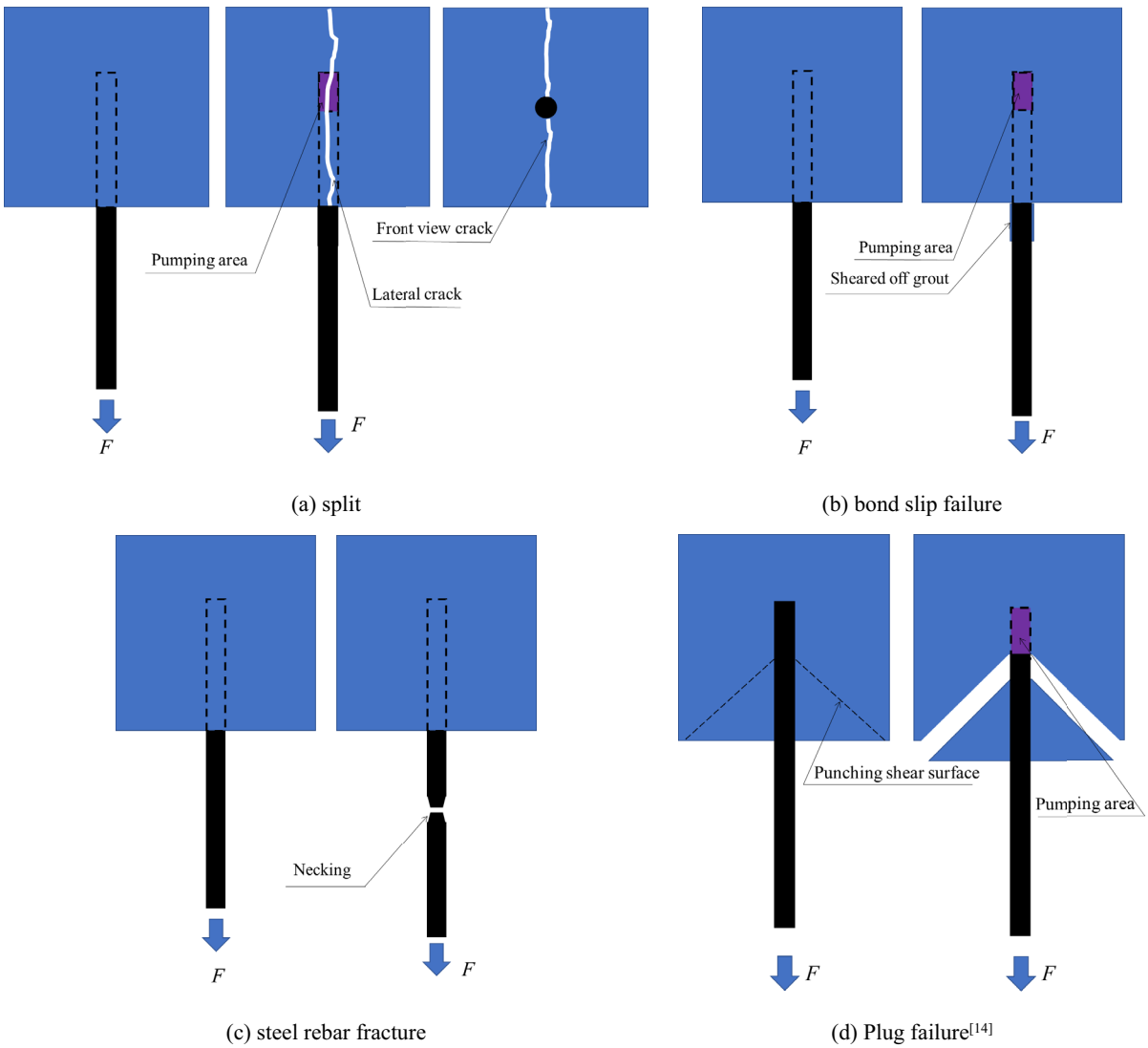

Fig. 4 Failure modes of pull-out tests.

Based on gel materials being disintegrated and leading to serious internal cracks in grout, Zhu et al. (2020) has found that residual compressive strength of grout specimens after exposed to 600 °C was about 27% of that at ambient temperature and bond behaviors decreased, which led to the steel rebar being pulled out of the sleeve from the steel rebar fracture outside of grouted sleeve connection at ambient temperature. Therefore, compared to the specimens at ambient temperature, it is safely concluded that the bond bearing capacity of the post-fire specimens decrease and failure modes will change to other types. Taken the reliability of specimens being decided by their failure modes into account, it is necessary to find out the critical temperature of failure modes changing, which is important to design the pull-out test specimens in the future and study the bond behaviors between grout and steel rebar.

3.2 Programs of the Test

Combined with the 27 specimens at ambient temperature by the author (Liu et al., 2021), there were three groups with nine specimens adding, i.e., 36 specimens, to investigate temperature effects on the mechanical behaviors of grout and steel rebar in present paper. It is well-known that 400 °C is the critical temperature when mechanical behaviors change for cementitious materials. In addition, it was found that the mechanical behaviors almost were the same as these at ambient temperature

Table 1 Design of the specimens.

Label	*d*/ mm	l_b (*d/ mm)	$f_{c,g}$/ MPa	Temperature/°C	Quantity
GBS 12-5d-500	12	5*d*/60	76.7	500	3
GBS 16-7d	16	7*d*/112	76.7	20	3
GBS 16-7d-500	16	7*d*/112	76.7	500	3

when the elevated temperature was no more than 400 °C, but changing to another state after the specimen was exposed to 600 °C (Liu et al., 2020; Xiao et al., 2009). Thus the elevated temperature with 500 °C was chosen to make sure the failure mode change occurring to the specimens in this paper. Features of specimens are listed in Table 1. Taking the specimen labeled GBS-12-5d-500 for example, GBS represents pull-out test, 12 is the steel rebar with diameter of 12 mm, 5d means 5 times diameter of steel rebar, and 500 is the specimen after exposed to 500 °C. In addition, d, l_b and $f_{c,g}$ represent diameter of steel rebar, embedment length of steel rebar and compressive strength of grout, respectively, in Table 1. The closed furnace with maximum temperature of 1000 °C and rated power of 36 kW was used to carry out the elevating test in Fire Safety of Engineering Structures Testing Division of State Laboratory for Disaster Reduction in Civil Engineering of Tongji University. The specimens were elevated to the target temperature of 105 °C firstly and 500 °C subsequently with heating rate of 5 °C/min, both of which were held for 120 min in the heating test. Then, the power switch was turned off and the specimens were not picked out until being cooled to ambient temperature to exert the loading test. The loading test was controlled by displacement and terminated after the displacement at free end of steel rebar up to 20 mm or the load declining to 0.3 times of the peak load. Moreover, the displacement at free end of steel rebar was collected by Linear Variable Differential Transformer as slip and the output force from the loading setup shown in Fig. 5 was regarded as load during the pull-out test.

Fig. 5 The loading setup.

3.3 Analysis on the Test Results

The grout cubic block with compressive strength of 76.7 MPa are kept completely, i.e., smooth surface and intact edges after heating up to 500 °C, but the surface color changes from general gray to gray white, as shown in Fig. 6. Therefore, explosive spalling of cement-based material with high compressive strength was inhibited during the heating process. According to the prementioned failure feature owning to the specimen after loading, it was found that there were two types failure modes of the specimens after loading. The steel rebar fracture and bond slip failure occur to specimens labeled GBS 16-7d and post-fire specimens labeled GBS 12-5d-500 and GBS 16-7d-500, respectively, as shown in Fig. 7, which means that the elevated temperature has obvious effect on the failure modes of pull-out test specimens. Taking the specimens GBS 16-7d and GBS 16-7d-500 for example, the failure mode changed from the steel rebar fracture to the bond slip failure after the specimens exposed to 500 °C.

Curves of load (F)–slip (s) are exhibited in Fig. 8a–c. It is found that the curves of specimens contain ascending and declining segments. The ascending segment characterized by linear development is nearly close to each other in the same group. The declining segment of specimen with the steel rebar fracture drops sharply after the curve of F–s up to the peak point as shown in Fig. 8a. However, the declining segment of specimen with the bond slip failure decreases slowly and nonlinearly beyond the peak point of the F–s curve, and then approaches to a horizontal line after the slip exceeding 5 mm as exhibited in Fig. 8b and c. The development of the horizontal line represents the classic feature that the load is balanced by the friction as bond strength of the specimen with bond slip failure. Taking the feature of F–s curves and the failure mode into account, it was found that post-fire specimens were the same to that, i.e., GBS 12-3d, GBS 16-4d and GBS 18-5d, etc., at ambient temperature from Liu et al. (2021). Therefore, the bond-slip constitutive relationship of post-fire specimens with bond slip failure is the same to that by Liu et al. (2021), as shown in Fig. 8d. In addition, the peak load and its corresponding slip and

(a) d=12mm (b) d=16mm

Fig. 6 Features of specimens after exposed to 500 ℃.

the residual load, namely, the load at the slip of 7.5 mm (Liu et al., 2021), are listed in Table 2.

Based on the peak loads from Table 2, the bond strength of specimen group was calculated by Eq. (1). Moreover, combined with the 27 specimens at ambient temperature (Liu et al., 2021), an expression has been built to calculate the bond strength including post-fire specimens by fitting analysis, which was listed as Eq. (2). The residual compressive strength of grout could be calculated by Eq. (3) from Zhu et al. (2020). The bond strength of specimen labeled GBS 16-7d is 25.1 MPa by the new built Eq. (2), which is higher than that test value of 20.6 MPa. The calculated result shows that the bond strength from test is the low limited value for the specimen with the steel rebar fracture, thus Eq. (2) is correct and feasible. In addition, it was found that the residual compressive strength from Eq. (3) should be enlarged 1.5 times to calculate the bond strength by Eq. (2) for simulation, which made the bearing capacity of specimens from simulation agreed with the test results well:

$$\tau = \frac{F}{\pi d l_{\mathrm{b}}}, \tag{1}$$

$$\frac{\tau_u}{\sqrt{f_{\mathrm{c,g}}^T}} = 32.805 \cdot d^{-0.415} \cdot l_{\mathrm{b}}^{-0.273}, \tag{2}$$

$$\frac{f_{\mathrm{c,g}}^T}{f_{\mathrm{c,g}}} = 18.88 + 0.78 \times \frac{f_{\mathrm{c,g}}}{1 + (T-20)^{3.95} \times 1.86 \times 10^{-10}}, \tag{3}$$

where τ and τ_u are bond stress and bond strength, respectively; F is the load output from the loading setup; d and l_{b} are diameter of steel rebar and its embedment length, respectively; $f_{\mathrm{c,g}}$ and $f_{\mathrm{c,g}}^T$ are compressive strength of grout at ambient temperature and after exposed to elevated temperature T, respectively; T is the elevated temperature. In addition, $f_{\mathrm{c,g}}^T$ could be from Eq. (3).

4 Simulation Analysis of Post-fire Specimens

4.1 Parameters for Analysis

The simulation analysis focused on the specimens labeled GBS 12-5d-500, GBS 16-7d and GBS 16-7d-500 firstly, and then the test results were used to verify the shape of F–s curves, peak load and failure mode from simulation analysis. Furthermore, taking the specimen with steel rebar diameter of 16 mm, i.e., d = 16 mm, and its embedment length of 6d, 7d and 8d, respectively, for example, a finite element simulation using the Abaqus soft was exerted to investigate the crucial temperature of failure mode change, which was important to design the pull-out test specimen and beneficial for the fire safety design of grouted sleeve connections.

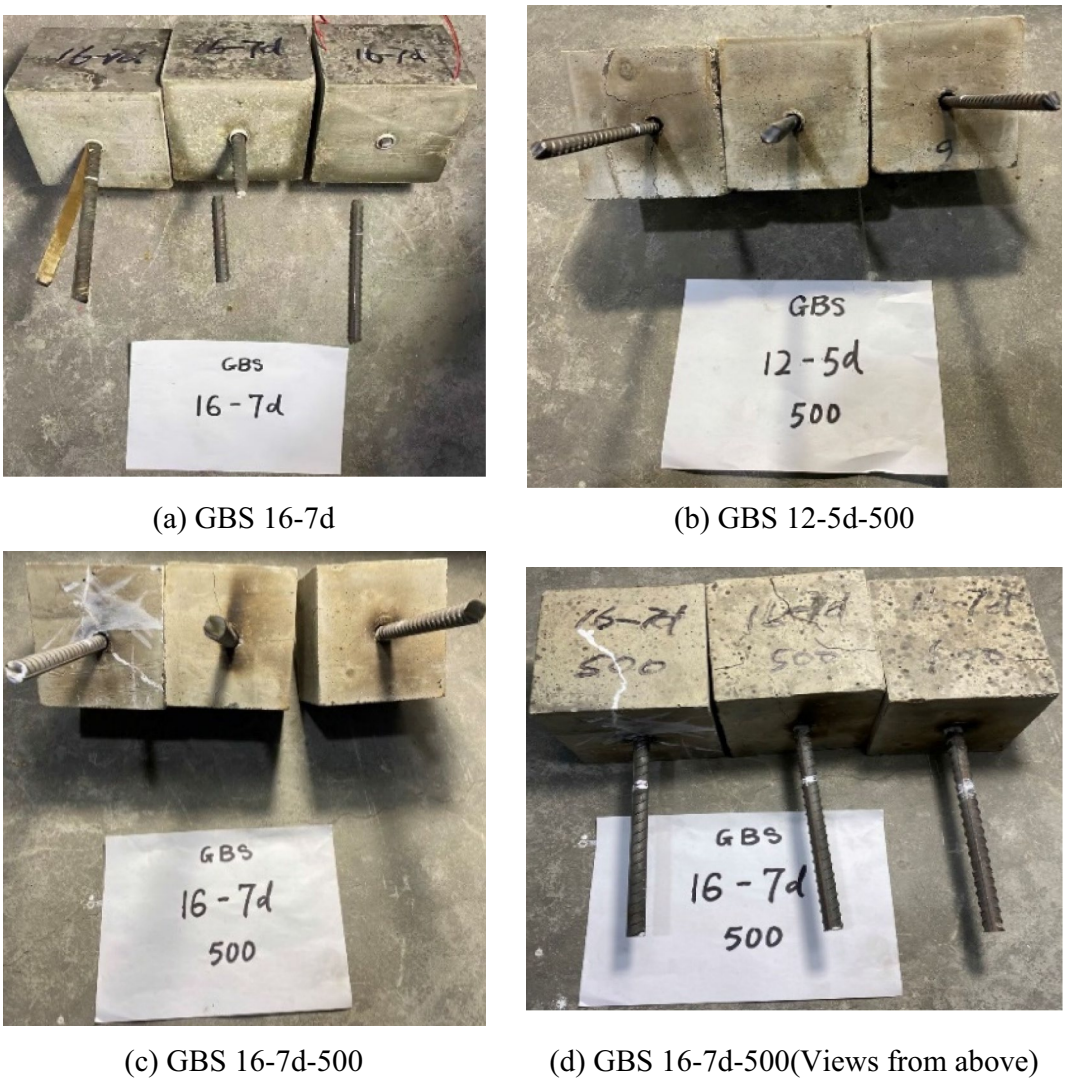

(a) GBS 16-7d (b) GBS 12-5d-500

(c) GBS 16-7d-500 (d) GBS 16-7d-500(Views from above)

Fig. 7 Types of failure modes.

4.2 FE Models for Simulation

FE models were created by Abaqus soft for the pull-out test specimens. The grout and steel rebar were simulated using the element characterized 8-node linear brick, reduced integration with hourglass control (C3D8R). The zero-thick 8-node three-dimensional cohesive element (COH3D8) with the traction–separation law was used to simulate interface between the grout and steel rebar. The compressive constitutive relationship of post-fire grout was from Liu et al. (2022) and the tensile constitutive relationship of post-fire grout was based on the same strength grade concrete in GB 50010-2010 (2015), which are listed in the first and third quadrants of coordinate system as shown in Fig. 9a. In addition, σ_c and σ_t are the peak stresses of grout under compression and tensile, and ε_{c0} and ε_{t0} are the strains corresponding to the peak stresses of grout under compression and tensile, respectively. Based on the test result data by Liu et al. (2022), the axial compressive constitutive relationship of post-fire grout and its coefficients are fitted into expressions (4), (5) and (6), respectively. The constitutive model of steel rebar is elastic–perfectly plastic model as shown in Fig. 9b, and f_y and ε_y are the yield strength and the corresponding strain of steel rebar. The yield strength and elastic modulus of post-fire steel rebar were calculated by the method supplied by Yu et al. (2005), which proposed that elastic modulus and yield strength of the steel rebar after exposed to up to 350 and 400 °C be the same to these values at ambient temperature, respectively,

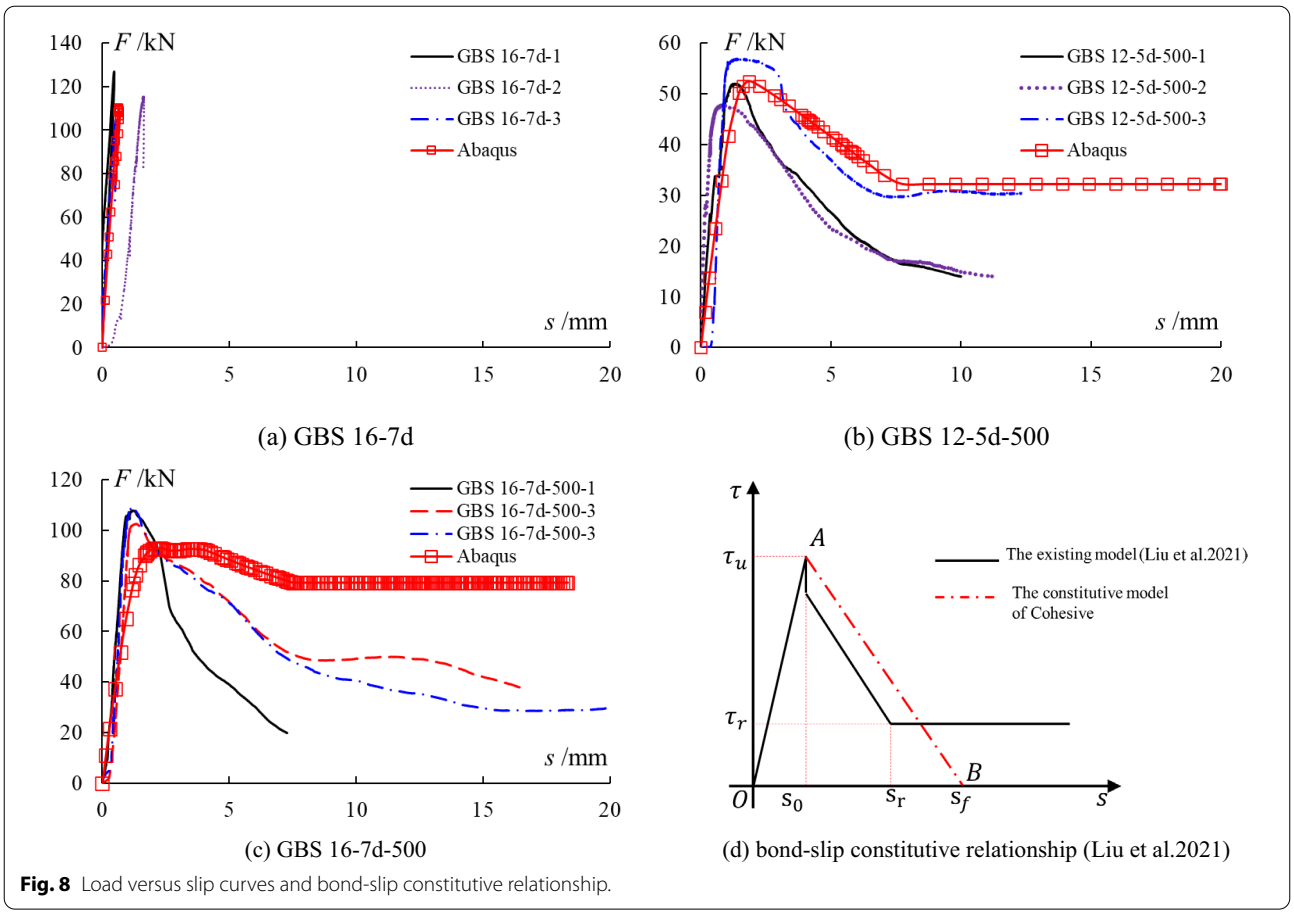

Fig. 8 Load versus slip curves and bond-slip constitutive relationship.

Table 2 Mechanical behavior parameters of specimens with the bond slip failure.

Label	Peak load (F_u)/kN		Peak slip(s_0)/mm		Residual load (F_r)/kN	
	Individuality	Average	Individuality	Average	Individuality	Average
GBS 12-5d 500	52.1	52.3	1.32	1.17	17.01	21.3
	47.9		0.83		17.23	
	56.9		1.36		29.78	
GBS 16-7d 500	107.8	106.4	1.18	1.22	19.93	39.7
	102.5		1.35		51.18	
	108.9		1.12		48.12	

and decrease along with the elevated temperature increasing. It is usually to use bi-linear model as the constitutive relationship of cohesive element (Teng et al., 2015; Xiao et al., 2021), which is shown in Fig. 8d. Moreover, the peak bond stress of the model is from Eq. (2) according to the design parameters of specimens. In addition, the peak slip s_0 corresponding to the peak stress was defined to be the same to the value at ambient temperature when the elevated temperature was no more than 400 °C and increased linearly as the elevated temperature beyond 400 °C (Xiao et al., 2014). Thus, the FE model is set up as shown in Fig. 10. It should be noted that the rectangle box behind the steel rebar is used to show the range of unbonded area between the steel rebar and grout, and the rebar in the unbonded area is deleted to speed the simulation analysis, as shown in Fig. 10b. Taking the specimen labeled GBS 12-5d-500 for example, the maximum size of

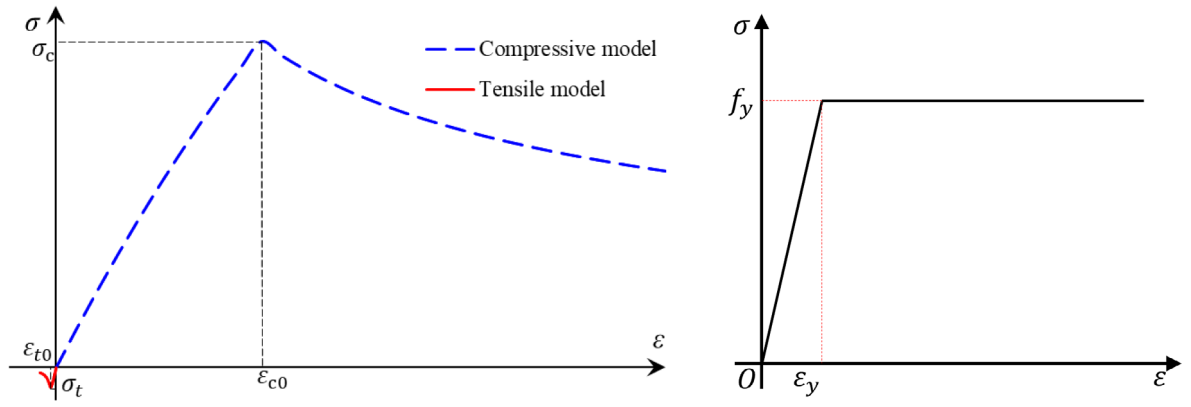

(a) grout (b) steel rebar

Fig. 9 Constitutive models of materials.

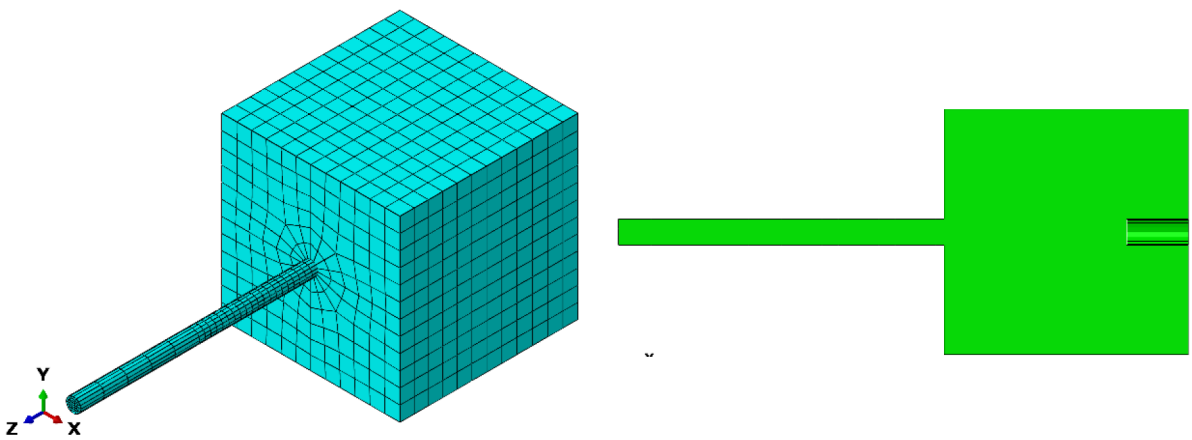

(a) Mesh (b) sectional drawing

Fig. 10 FE model for simulation analysis.

element is 20 mm and the total element is 3440, and the FE model is shown in Fig. 10a.

$$y = \begin{cases} ax^2 + bx & x \le 1.0 \\ x^c & x \ge 1.0 \end{cases}, \tag{4}$$

$$\begin{cases} a = 0.0006T - 0.2376 \\ b = -0.0006T + 1.2376 \\ c = -0.0007T - 0.4842 \end{cases}, \tag{5}$$

$$\frac{E_g^T}{E_g} = -0.146\ln T + 1.4355, \tag{6}$$

where a, b and c are the coefficients of axial compression constitutive model for post-fire grout (Liu et al., 2022); ε divided by ε_{0T} is x and σ divided by σ_{uT} is y; σ and ε are stress and strain; σ_{uT} and ε_{0T} are peak stress and its strain; E_g and E_g^T are the elastic modulus of grout at ambient temperature and after exposed to elevated temperature; T is the elevated temperature.

4.3 Verification

Curves of F–s named Abaqus are added to Fig. 8a–c and the failure features from simulation specimens are shown in Fig. 11. It is found that shapes of F–s curves from simulation are similar to these test curves and the ascending segments are consistent to each other well. In addition,

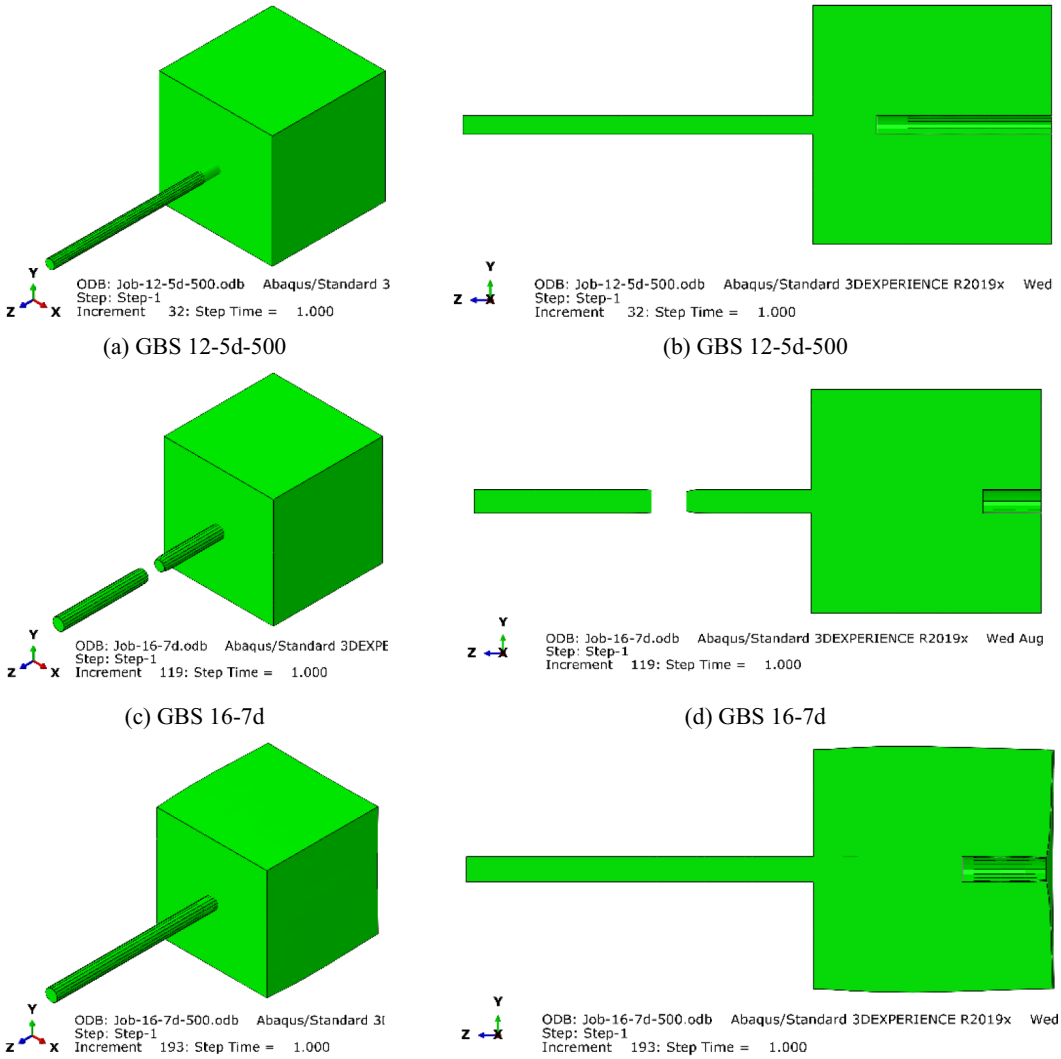

Fig. 11 Failure features of simulation specimens.

peak loads of simulation specimens labeled GBS 12-5d-500, GBS 16-7d and GBS 16-7d-500 are generally lower than these test results, i.e., 1.004, 0.952, 0.873 times of the latter, which shows that the simulation result is prone to safety. According to Fig. 11d, it is found that the rectangle box area behind steel rebar of specimen labeled GBS 16-7d is the same to that shown in Fig. 10b, which means that there is no slip between steel rebar and grout occurring to the simulation specimen labeled GBS 16-7d with the steel rebar fracture. However, ranges of rectangle boxes of simulation specimens labeled GBS 12-5d-500 and GBS 16-7d-500 become larger than that shown in Fig. 10b in longitudinal direction, and the enlarge area has smooth surface, which means that a relative displacement, i.e., slip, occurs to the interface between grout and steel rebar. In addition, the steel rebar still remains intactness when the loading process is completed. Therefore, it is safe to conclude that the bond slip failure occurs to the simulation specimens labeled GBS 12-5d-500 and GBS 16-7d-500. Finally, it is found that the failure modes of simulation specimens labeled GBS 16-7d, GBS 12-5d-500 and GBS 16-7d-500 are the same to these test results. Combined with the *F*–*s* curves, peak loads and failure modes of simulation analysis, it can be safely concluded that the simulation method is feasibility and correct. In addition, the rectangle box behind steel rebar shape is an important index to distinguish the failure modes of pull-out test specimens.

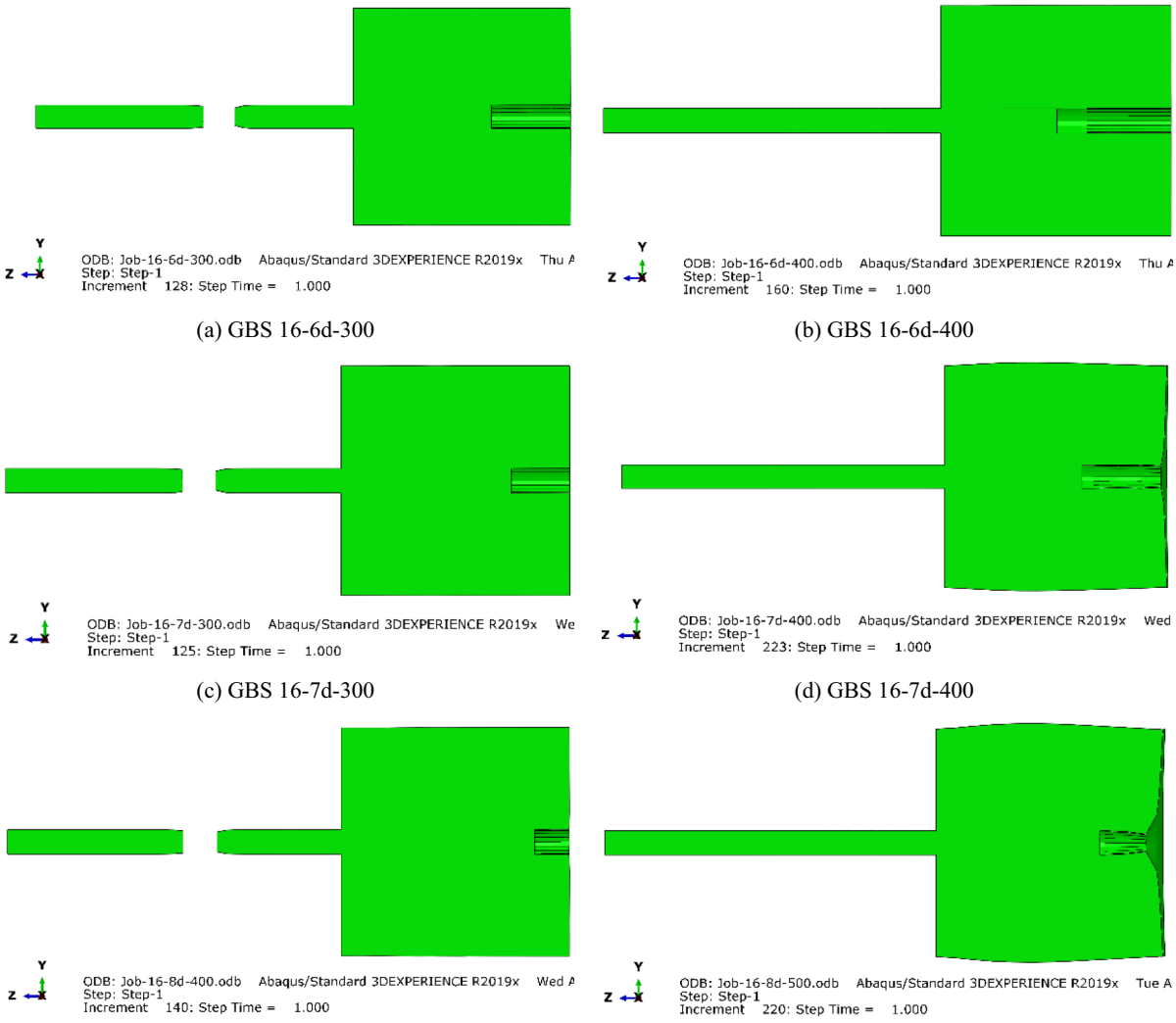

Fig. 12 Failure features of simulation specimens.

4.4 Varying Parameters in Simulation Analysis

Taking the specimens with steel rebar diameter of 16 mm ($d=16$ mm) and embedment lengths of 6d, 7d and 8d ($l_b=6d$, 7d and 8d) as research objects, the effects of elevated temperature up to 500 °C on bond behaviors were investigated by simulation analysis on pull-out test specimens. Failure features and F–s curves of simulation specimens are exhibited in Figs. 12 and 13, respectively. It is found that the steel rebar fracture occurs to the simulation specimens labeled GBS 16-6d-300, GBS 16-7d-300 and GBS 16-8d-400 as shown in Fig. 12a, c and e. Ranges of rectangle boxes are enlarged and the enlarged part is smooth in the simulation specimens labeled GBS 16-6d-400, GBS 16-7d-400 and GBS 16-8d-500, which means that slips occur to the interface between grout and steel rebar. According to Fig. 13d, F–s curves of the simulation specimens labeled GBS 16-6d-400, GBS 16-7d-400 and GBS 16-8d-500 are similar to the test results of specimens labeled GBS 12-5d-500 and GBS 16-7d-500 shown in Fig. 8b and c. Therefore, combined with the steel rebar intact, it can be concluded that the bond slip failure happens to the simulation specimens labeled GBS 16-6d-400, GBS 16-7d-400 and GBS 16-8d-500. Consequently, it is proposed that the crucial temperatures of failure mode change be 300, 300 and 400 °C for pull-out specimens with steel rebar diameter of 16 mm ($d=16$ mm) and embedment lengths of 6d, 7d and 8d ($l_b=6d$, 7d and 8d), respectively, which means that the failure mode of specimens will change from the steel

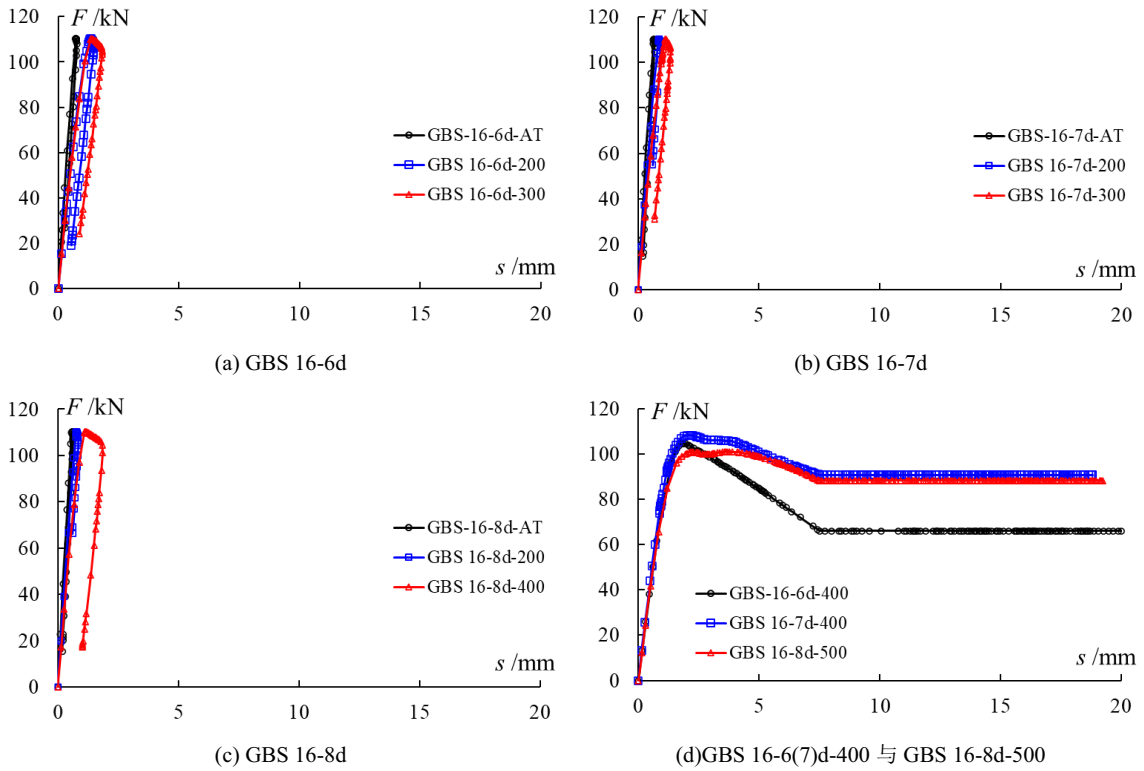

Fig. 13 *F–s* curves of simulation specimens.

rebar fracture to the bond slip failure when the elevated temperature exceeds the crucial temperature.

5 Conclusions

The bond behaviors between grout and steel rebar were investigated by theory analysis, the pull-out test and finite element simulation, which focused on the elevated temperature effects in present paper. The results and suggestions are as follows:

1. Force mechanism of interface is brought out by the bond action between grout and steel rebar, and the failure modes mainly contain three types, namely, the split, the steel rebar fracture and the bond slip failure. Taken the loading regime, compressive strength of grout and lateral restraint into account, plug failure may occur to specimens of pull-out tests.
2. Combined with pre-drying 120 min at 105 °C and the low heating rate with 5 °C/min, explosive spalling of high-strength grout (76.7 MPa) is inhibited during the heating test with maximum temperature of 500 °C.
3. At ambient temperature, the steel rebar fracture occurs to specimens labeled GBS 12-5d and GBS 16-7d in the pull-out test, but the failure mode of specimens labeled GBS 12-5d-500 and GBS 16-7d-500 is the bond slip failure.
4. Based on the effects of the elevated temperature, compressive strength of grout, diameter and embedment length of steel rebar, an equation of bond strength between grout and steel rebar for post-fire specimens is built by fitting analysis of the data from test.
5. The full failure process of rebar fracture could be captured by simulation analysis, which is the important sign to distinguish the failure mode of specimens.
6. It is proposed that the crucial temperature of failure mode change be 300, 300 and 400 °C for the pull-out test specimens with embedment length of 6*d*, 7*d* and 8*d*, respectively.

Acknowledgements

The authors wish to acknowledge the financial support from the Science and Technology Planning Project of Jiangxi Education Department in China (GJJ201010) and the general support from Professor Jian-Zhuang Xiao of Tongji University.

Author contributions
L-LL was a major contributor in writing the manuscript, C-YL carried out the investigation of testing method, L-XO was a major contributor of the data analyzation, Z-HX was a major contributor of test, W-HL was a major contributor of simulation. All authors read and approved the final manuscript.

Authors' information
Liang-Lin Liu is a lecturer at the School of Architecture and Civil Engineering, Jinggangshan University, Ji'an, Jiangxi, 343009, China. Chun-Yong Luo is a vice professor at the School of Architecture and Civil Engineering, Jinggangshan University, Ji'an, Jiangxi, 343009, China. Lu-Xia Ouyang is a lecturer at the School of Architecture and Civil Engineering, Jinggangshan University, Ji'an, Jiangxi, 343009, China. Zhen-Hua Xia is a lecturer at the School of Architecture and Civil Engineering, Jinggangshan University, Ji'an, Jiangxi, 343009, China. Wei-Hua Li is a lecturer at the School of Architecture and Civil Engineering, Jinggangshan University, Ji'an, Jiangxi, 343009, China.

Funding
Science and Technology Planning Project of Jiangxi Education Department in China (GJJ201010).

Availability of data and materials
All data generated or analyzed during this study are included in this article.

Declarations

Ethics approval and consent to participate
Not applicable.

Consent for publication
Not applicable.

Competing interests
The authors declare that they have no competing interests.

Received: 12 November 2021 Accepted: 10 April 2022
Published online: 27 June 2022

References

Eligehausen, R., Popov, E. P., & Bertero, V. V. (1983). *Local bond stress-slip relationships of deformed bars under generalized excitations*. University of California.
GB 50010-2010 (2015 Edition). (2015). Code for design of concrete structures. Beijing: China Architecture and Building Press. in Chinese.
Hosseini, S. A., & Rahman, A. B. A. (2016). Effects of spiral confinement to the bond behavior of deformed reinforcement bars subjected to axial tension. *Engineering Structures, 112*, 1–13.
Kim, H. K. (2012). Bond strength of mortar-filled steel pipe splices reflecting confining effect. *Journal of Asian Architecture and Building Engineering, 11*(1), 125–132.
Li, J., Gao, X. L., & Ai, X. Q. (2004). The bond properties between fiber-reinforced concrete and deformed bar. *Journal of Building Structures, 25*(1), 99–103. in Chinese.
Ling, J. H., Rahman, A. B. A., Mirasa, A. K., et al. (2008). Performance of CS-sleeve under direct tensile load: Part I: Failure modes. *Malaysian Journal of Civil Engineering, 20*(1), 89–106.
Liu, L. L., Xiao, J. Z., Ding, T., et al. (2020). Experimental study on mechanical behavior of thermally damaged grouted sleeve splice under cyclic loading. *Structural Concrete, 21*(6), 2494–2514.
Liu, L. L., Xiao, J. Z., Ding, T., et al. (2021). Test and simulation on bond behavior between sleeve grout and high strength steel rebar. *Journal of Tongji University (natural Science), 49*(9), 1275–1283. in Chinese.
Liu L. L., Xiao J. Z., Li J. X., et al. (2022). Static and dynamic mechanical behaviors of heat-damaged cementitious grout under uniaxial compression loadings. *Advanced Engineering Sciences*. in Chinese, in Press.
Tastanil, S. P., & Pantazopoulou, S. J. (2010). Direct tension pullout bond test: Experimental results. *Journal of Structural Engineering, 136*(6), 731–743.
Teng, J. G., Fernando, D., & Yu, T. (2015). Finite element modelling of debonding failures in steel beams flexurally strengthened with CFRP laminates. *Engineering Structures, 86*, 213–224.
Xiao, J. Z., Hou, Y. Z., & Huang, Z. F. (2014). Beam test on bond behavior between high-grade rebar and high-strength concrete after elevated temperatures. *Fire Safety Journal, 69*, 23–35.
Xiao, J. Z., Huang, J. L., & Zhao, Y. (2009). On bond behavior between HPC and fine grain steel bar after elevated temperatures. *Journal of Tongji University (natural Science), 37*(10), 1296–1301. in Chinese.
Xiao, J. Z., Liu, H. R., & Ding, T. (2021). Finite element analysis on the anisotropic behavior of 3D printed concrete under compression and flexure. *Additive Manufacturing, 39*, 101712.
Xu, F., Wu, Z. M., Zheng, J. J., et al. (2012). Experimental study on the bond behavior of reinforcing bars embedded in concrete subjected to lateral pressure. *Journal of Materials in Civil Engineering, 24*(1), 125–133.
Yu, Z. W., Wang, Z. Q., & Shi, Z. F. (2005). Experimental research on material properties of new III grade steel rebar after fire. *Journal of Building Structures, 26*(2), 112–116. in Chinese.
Zhang, W. X., Deng, X., Zhang, J. Y., et al. (2018). Tensile behavior of half grouted sleeve connection at elevated temperatures. *Construction and Building Materials, 176*, 259–270.
Zheng, Y. F., Guo, Z. X., Liu, J. B., et al. (2016). Performance and confining mechanism of grouted deformed pipe splice under tensile load. *Advances in Structural Engineering, 19*(1), 86–103.
Zhou, Y. H., Ou, Y. C., & Lee, G. C. (2017). Bond-slip responses of stainless reinforcing bars in grouted ducts. *Engineering Structures, 141*, 651–665.
Zhu, J. N., Guo, D. D., Ma, J. F., et al. (2020). Experimental study on tensile properties of semi-grouting sleeve after high temperature. *Engineering Mechanics, 37*(5), 104–111. (in Chinese).
Zhu, J. N., Ma, J. F., Guo, D. D., et al. (2021). Study on tensile properties of semi grouted sleeve connectors after high temperature. *Construction and Building Materials, 302*, 124088.

Publisher's Note